Available online at www.sciencedirect.com

ScienceDirect

Advances in Space Research 67 (2021) 1468–1476

ADVANCES IN SPACE RESEARCH (a COSPAR publication)

www.elsevier.com/locate/asr

Material selection for a CubeSat structural bus complying with debris mitigation

Emanuele A. Slejko [a,c,*], Anna Gregorio [b,c], Vanni Lughi [a]

[a] Department of Engineering and Architecture, University of Trieste, Via Alfonso Valerio 6/1, 34127 Trieste, Italy
[b] Department of Physics, University of Trieste, Via Alfonso Valerio 2, 34127 Trieste, Italy
[c] PICOSATS srl, Area Science Park, Padriciano 99, 34149 Trieste, Italy

Received 18 August 2020; received in revised form 4 November 2020; accepted 30 November 2020
Available online 24 December 2020

Abstract

The increasing number of commercial, technological and scientific missions for CubeSats poses several concerns about the topic of space junk and debris mitigation. As no regulation is currently in place, innovative solutions are needed to mitigate the impact that Low Earth Orbit objects can have during uncontrolled re-entry and the associated potential events of surface collision. We investigated the requirements, in terms of materials selection, for the development of a 3D-printed structural bus able to withstand loads during launch and in-orbit operations, with the objectives to be as light as possible and requiring the least amount of heat for demise during atmospheric re-entry. The selection indicated magnesium alloys as the best candidates to improve the reference material, aluminium 6061 T6, resulting in both mass-reduction and improved demisability. We also analysed how the relative importance of these two objectives can modify the selection of materials: if minimizing the heat to disintegration were valued more highly than lightness, for example, the new best candidates would become tin alloys. Our analysis, furthermore, suggested the importance of Liquid Crystal Polymer as the sole plastic material approaching the performance of the best metal choices. This contribution, thus, provides novel insight in the field of 3D-printed materials for the fast-growing CubeSat segment, complying with the debris mitigation initiatives promoted by space agencies and institutions.

Keywords: CubeSat; Materials selection; Debris mitigation; Magnesium alloys; Sustainability

1. Introduction

CubeSats are a specific type of small satellites, first introduced in the late '90 by CalTech, characterised by modular elements of dimensions 10x10x10 cm^3 (California Polytechnic State University, 2014). Several CubeSat units can be combined together to fit the volume requirements of the payload: nowadays, common form-factors are 3-unit or 6-unit combinations (conventionally labelled as 3U and 6U, respectively). CubeSats have captured the attention of national and international space agencies thanks to their cost-effective approach, related to the use of commercial off-the-shelf components, and fast development time, while maintaining high-performance thanks to the progress in the miniaturization of electronic and optical components (Shiroma et al., 2011; Sweeting, 2018; Toorian et al., 2008; Woellert et al., 2011). As space is becoming ever more commercial-oriented, with plans for massive small-satellite constellations by private companies such as for example SpaceX with the StarLink program, CubeSats are gaining a prominent role in the Telecommunication and Earth Observation/Remote Sensing sector of

* Corresponding author at: Department of Engineering and Architecture, University of Trieste, Via Alfonso Valerio 6/1, 34127 Trieste, Italy.
E-mail address: easlejko@units.it (E.A. Slejko).

https://doi.org/10.1016/j.asr.2020.11.037
0273-1177/

the industry (Akyildiz and Kak, 2019; Burleigh et al., 2019; Peral et al., 2018; Selva and Krejci, 2012). Moreover, CubeSats maintain a role as scientific means to investigate the effect of microgravity and outer-space conditions, or to carry out space exploration – like for example NASA's O/OREOS and MarCO missions (Ehrenfreund et al., 2014; Schoolcraft et al., 2016). However, with the increasing number of spacecrafts orbiting Low Earth Orbit - LEO, i.e. orbits with an altitude within 2000 km from Earth's surface (Inter-Agency Space Debris Coordination Committee, 2007) - concerns are arising related to space debris and space junk in general (Murtaza et al., 2020). The altitude of LEO objects reduces with time due to atmospheric drag, ultimately re-entering the atmosphere and potentially impacting the ground. Standard procedures for the end-of-life disposal and re-entry of small satellites could benefit the management of the space debris problem. Research is being conducted to address this issue and propose solutions compliant to "Clean Space" initiative and Debris Mitigation plans promoted by space agencies. However, as no actual regulation has been established at this moment, these solutions are seldom applied in a consistent way, except for sporadic missions and technology demonstrators (Carandente and Savino, 2014; Hakima et al., 2018; Murtaza et al., 2020). ReDSHIFT is one example of a project aimed at the development of passive means to reduce the impact of space debris, recurring to 3D-printed plastic structures for the development of a small satellite (Rossi et al., 2019, 2018). The project represents one of the most notable efforts to address the space debris challenge, with the intention to raise the readiness level of the Design for Demise approach.

In this contribution, we propose an advanced yet cost-effective solution to mitigate the problem of space debris. The structural bus of a CubeSat is generally made of aluminium 6061 T6 or 7075 T6 because of ease of fabrication, low cost, and excellent mechanical properties that guarantee they withstand the stresses imposed during all the phases of a space mission - schematically synthesized in Fig. 1. The high heat-to-decomposition of these materials, however, represents a barrier for thermal decomposition of the CubeSat structure and paylod during uncontrolled atmospheric re-entry (Bastida Virgili et al., 2016; Klinkrad et al., 2004). In this contribution, aluminium 6061 T6 has been selected as reference material for our discussion, because it presents lower mechanical properties than aluminium 7075 T6, yet still exceeding the ones required for the application. Substituting aluminium with another material presenting a combination of low melting point, low specific heat capacity, and low latent heat of fusion would lead to complete demise of the structural frame in a shorter time, thus securing a larger amount of heat for the degradation of other critical components like steel spacer rods and reaction wheels, for example. Design to demise might also require the release of critical components upon failure of the structure, as an effective solution to promote the degradation of such equipment. Another important aspect of the material selection is related to its formability by 3D-printing, which is acquiring considerable importance in the development of optimized structures or integrated parts (Espalin et al., 2014; Gaudenzi et al., 2018). In fact, the International Space Station already operates a 3D-printer in one of its modules. It is expected that the future efforts to colonize the Moon and Mars will require this technology to avoid the production of space equipment on Earth, with the associated technological obstacles and economical limitations related to the launch of complete and finalized space systems from our planet (Prater et al., 2017). Production in-orbit or on the surface of other planets is a much-needed capacity for accelerating the exploration and colonisation of the Solar System; therefore the development of novel structural and functional materials for 3D-printing is a fundamental step in this direction.

As the state of the art does not consider the aspects mentioned above, since aluminium 6061 cannot be 3D printed and the heat to decomposition has never been a major objective for the selection of this material, we decided to focus our attention on innovative solutions that have not been fully exploited yet in aerospace applications. We

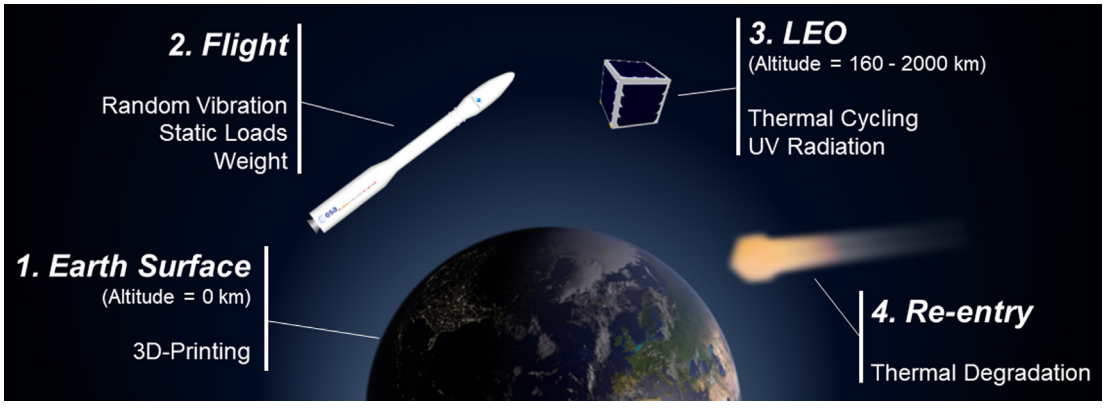

Fig. 1. Material's requirements for the development of a CubeSat structural bus considered in this research, categorized by deployment stages from Earth preparation to in-orbit operations and uncontrolled re-entry.

identified specific families of metals and polymers as best candidates. These materials are not entirely new to aerospace applications, although their use is currently limited to only a few non-critical components. However, they represent valid alternatives to address incumbent challenges arising in this sector, and a shift from an occasional to a systematic use is desirable. The recent and continuous advances in 3D printing are a key and timely enabler for such a shift (Chen et al., 2014; Grim et al., 2016; Gutierrez et al., 2011; Piattoni et al., 2012; Straub et al., 2015).

Therefore, objective of this contribution is to propose new candidates to extend the pool of materials for aerospace applications and exploit the impact that innovative solutions can have in such technologically advanced fields and hostile environments. In detail, the main objectives of our analysis are related to:

- a reduction of mass, as the cost to launch to space is proportional to the mass of the system and it represents the greatest fraction of the total cost;
- the ability to demise faster compared to standard aluminium, coherently to the debris mitigation rationale discussed above.

2. Material and methods

The logic followed during the selection process is based on two major steps:

- Identify the profile of material attributes that best meets the requirements of the design (screening step).
- Compare this desired profile with the attribute profiles of available engineering materials to find the best match (ranking step).

Constraints and constrained objectives are expressed in mathematical form as a function of geometrical, functional, and materials parameters. The materials-dependent portions of these functions (i.e. the *materials indexes*) are used to screen and rank the materials. A graphical approach is used here: materials indexes charts are plotted, where the best candidates are easily detected among all the possible options. The objective represents the performance criterion that the best material maximizes (or minimizes, depending on the context). The selection process can be performed manually as well as by computational tools. Since we aimed at performing a deep evaluation and analysis of available choices for the project, a computer-aided procedure has been followed. The software utilised for the task at hand is CES Selector 2018 Polymer Edition by Granta®, which provides a comprehensive database of material properties.

Design requirements for a CubeSat structure, and for any design project in general, can be subdivided in three different categories: function, constraints and objectives. The function is straightforward: the need is to design a cubic frame containing the payload for a CubeSat. The frame has to withstand all mechanical and thermal loads during launch and in-orbit operations (F001). For the specific case of a CubeSat structural bus, the major modes of loading due to static loads and random vibration during launch are buckling and bending, illustrated in Fig. 2 (Okolie et al., 2016; Quiroz-Garfias et al., 2007). Identifying the appropriate modes of loading is important, as the main function for the considered system is to preserve its integrity and the one of the payload.

Since we are interested in a general approach, without any mission-specific requirements, we took as a reference the current available aerospace standards, particularly the NASA and ECSS standard frameworks (European Cooperation for Space Standardization, 2012; NASA Goddard Space Flight Center, 2013) and the CubeSat Design Specification standard (California Polytechnic State University, 2014). Table 1 indicates the main constraints related to the project with their associated acceptable values. We identified eight different constraints, related to mechanical, thermal and production aspects. More details about each constraint are provided in Supporting Information, where the rationale for the calculation of threshold values is also specified.

The constraints are identified in order to address the major design requirements of the structural bus, such as:

- The materials properties shall not degrade under solar radiation.
- The structural bus is subjected to the thermal environment, with temperature cycles and resulting dilatation or shrinkage. The material shall operate without failure in the temperature window of −20 to +80 °C (Kang and Oh, 2016; Piattoni et al., 2012; Stevenson Soler Chisabas et al., 2017), with a maximum thermal expansion coefficient of 100 μstrain/°C.
- The materials shell be produced by additive manufacturing.
- Since the structure main function is to protect and contain the payload, we want it to withstand the mechanical stresses during launch and in-orbit operation. This is expressed by the acceptable values for Young modulus and yield strength of the material (Barsoum et al., 2019; European Cooperation for Space Standardization, 2008; Okolie et al., 2016).

Considering all the above project constraints, a shortlist of potential candidates is obtained, as all the materials that do not comply with the requirements are eliminated (screening phase based on constraints). We furthermore opted for a stiffness-limited design rather than a strength-limited design, as the expected loads are too weak to cause failure of the materials. In the stiffness-limited approach, our intention is to avoid excessive elastic deformation of the spacecraft, which would potentially cause damage to the internal payload. All the considerations explained so

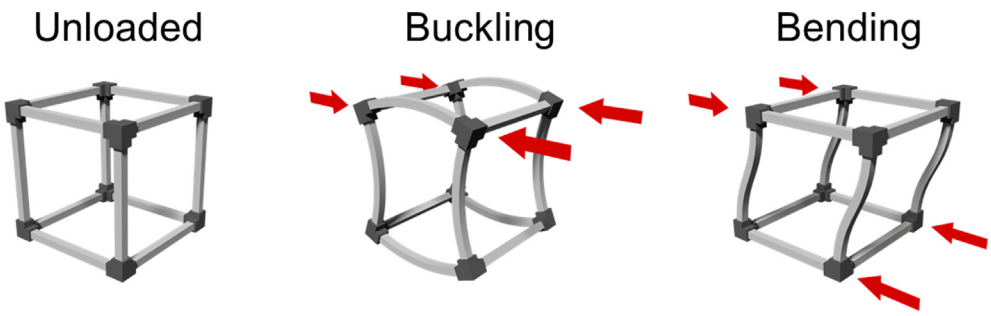

Fig. 2. Modes of loading considered in this research for a CubeSat structural bus. Buckling and bending are the two modes of loading that most significantly contribute to the failure of CubeSat structures subjected to static loads and random vibration.

Table 1
Component constraints defined in this research: the requirements are linked to materials attributes and accepted values are specified so that all candidates not satisfying these conditions are discarded. Accepted values are explained in Supporting Information.

Constraint ID	Description	Material Attribute	Accepted Value
C001	Shall not degrade under unshielded solar irradiance	UV Radiation Resistance	Excellent, Good
C002	Shall not deform too much due to thermal cycling	Thermal Expansion Coefficient	≤0.0001 strain/°C
C003	Shall be able to withstand orbital temperature cycles	Maximum Service Temperature	≥+80 °C
C004		Minimum Service Temperature	≤−20 °C
C005	Shall be produced by 3D printing	Production Process	Additive Manufacturing
C006		% Filler	0%
C007	Shall not fail under loads	Yield Strength	≥5.1 MPa
C008		Elastic Modulus	≥2.5 GPa

Table 2
Function, constraints, objectives and free variables for the materials design of the aerospace structure considered in this research.

Design Requirement	Description
Function	Structural bus
Constraints	UV radiation, thermal expansion, service temperature, production process, loads
Objectives	Minimise mass and heat for melting
Free Variables	Choice of material and beam section

far are summarised in Table 2, which presents the design requirements for a light, stiff and easily demised structure for aerospace applications. The objectives of the project are to produce a structure that is as light as possible (X001) and be able to demise requiring as little heat as possible (X002). To evaluate the best candidates in the shortlist, objectives are formulated in the form of performance equations, as follows.

$$m = \rho L A$$

$$\int_0^t (\dot{q_{in}} - \dot{q_{out}})dt = \int_{T_0}^{T_f} c_p(T) m dT + m\lambda_m$$

In the first performance equation the mass m of the element is expressed as a function of the density ρ, the length L (fixed) and the section area A (free variable). In the second equation $\dot{q_{in}}$ is the generated heat rate due to drag during re-entry, $\dot{q_{out}}$ is the thermal radiation rate, $c_p(T)$ is the specific heat capacity of the material, λ_m is the latent heat of melting. T_0 and T_f are the initial and final temperatures: in our analysis, the final temperature is equal to the melting point of the material. It has been demonstrated how the emitted radiation has considerable importance as its effect is to reduce the net incoming heat towards the system (Beck et al., 2019). During re-entry, modifications on the surface of the materials take place, influencing the emissivity of the component. For example, the aluminium surface can undergo oxidation, increasing its emissivity by one order of magnitude. Another important factor in the emitted radiation is the melting temperature of the material: the higher the melting point, the longer it will require to demise the component, resulting in a larger fraction of heat lost due to thermal radiation. With our general approach, it is impossible to quantify the change in emissivity for every single material. We have recurred to a simplified equation where the radiated heat is not considered, an approach already used in other studies (Kelley and Jarkey, 2015).

The two performance equations, combined with the failure modes of the system (see Supporting Information for detailed calculation), depend upon the two material indexes $M1$ and $M2$, where E represents the elastic modulus of the material

$$M1 = \frac{\rho}{E^{1/2}}$$

$$M2 = \left[\left(\frac{\rho c_p (T_f - T_0)}{E^{\frac{1}{2}}}\right) + \left(\frac{\rho \lambda_m}{E^{\frac{1}{2}}}\right)\right]$$

The best candidates, in absolute terms, will be the ones that minimize simultaneously these two material indexes.

3. Result and discussion

By applying the constraints of Table 1 to the CES Selector® - Polymers Edition database, consisting initially of more than 6000 materials, we obtained a shortlist of 399 potential solutions. All these materials can successfully carry out the function we defined, complying with the previously identified constraints. Among these, some are expected to perform better than others, meaning that they can weigh less and/or demise faster. Material indexes help us identify the best options; in a graphical approach (Fig. 3), *M1* and *M2* are the coordinates in a *materials property chart*, and each material is represented by a point (or a bubble, to allow for variability in the material properties). The closer a material is located to the origin of the axes, the lower the indexes, and therefore the best its performance. Fig. 3a indicates several materials belonging to the shortlist of potential candidates; among them, the lowest values of *M1* and *M2* are displayed by magnesium alloys (smallest *M1*) and tin alloys (minimum *M2*). In general, there is not an absolute best choice, i.e. a choice simultaneously presenting a combination of the lowest *M1* and *M2*. Rather, it is possible to identify a Pareto front – a subset of non-dominated choices of material (i.e. choices that cannot be outperformed by any other choice in terms of both objectives simultaneously). Fig. 3b indicates the position of the reference aluminium 6061 T6 in the chart. This plot has been subdivided in four areas by straight dashed lines corresponding to the values of the indexes for the reference. The top-right area contains materials that are heavier and require more heat to demise than aluminium 6061; this area is of no interest for our analysis. The top-left and bottom-right areas present materials that are lighter but less demisable or heavier but more demisable, respectively. The bottom-left area displays materials that are better than the reference in terms of both indexes. Magnesium alloys are located in this area. Note that aluminium is indeed considered a demise-friendly material, as its index M2 is lower than many other candidates thanks to the high enthalpy measured in wind tunnel tests (Beck et al., 2019; Kelley and Jarkey, 2015). Nevertheless, it represents a sub-optimal choice, since other candidates can behave comparably or even better in terms of demisability, without disadvantages in terms of weight and mechanical strength.

One material of particular interest is Liquid Crystal Polymer (LCP). It belongs to the bottom-right area of the plot, as it presents a *M1* index slightly larger than aluminium 6061, but lower *M2*. It is the only polymeric material close to the best candidates; other polymeric materials often considered as high performing, such as Polyoxymethylene (POM), Polyetherimide (PEI) and Polyether Ether Ketone (PEEK), have M1 and M2 indexes markedly larger than the reference material. LCP, while not presenting the best attributes for the objectives of this analysis, is nevertheless quite interesting for its excellent properties, and deserves consideration 'due to the fact that it is possible to produce LCP components by additive manufacturing, and specificaly by Fused Deposition Modelling (FDM).

The superior properties of printed LCP are related to the directional orientation of its molecular domains during printing, forming a hierarchical structure which possesses stiffness, strength and toughness comparable to lightweight composites (Gantenbein et al., 2018). It is reported that, thanks to the microstructural control during fabrication, its mechanical properties are larger than unfilled PEEK,

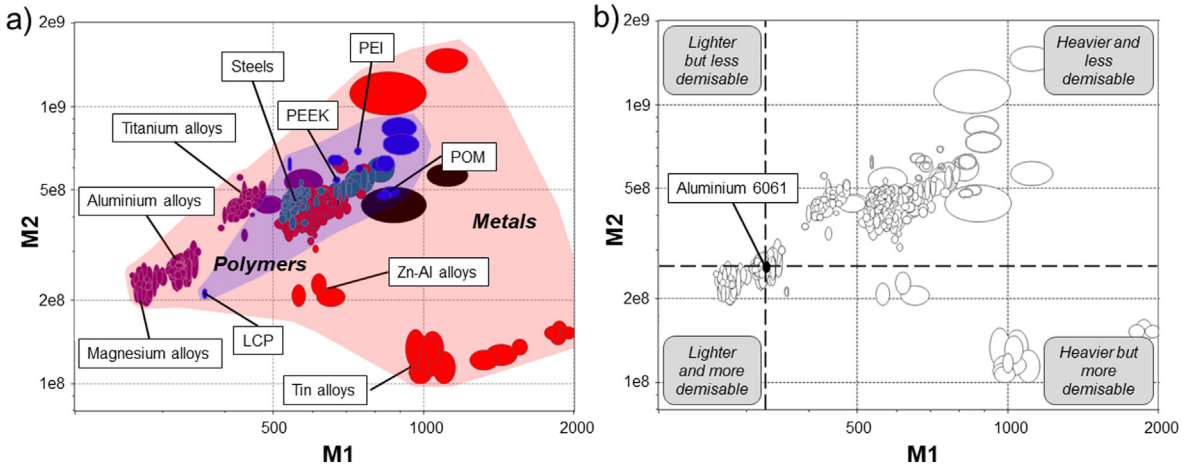

Fig. 3. Materials property charts based on the identified material indexes M1 and M2 described in the text. a) Each bubble refers to a specific material, and different colours indicate different material families. The two envelopes are labelled based on the material they represent: Metals and Polymers. b) The reference material (Al 6061) has been emphasized in the plot. Depending on combinations of material indexes relative to the reference, four different areas can be defined. The area of interest is the bottom-left one, where materials lighter and more demisable than aluminium 6061 can be found.

which is currently adopted as high-performance polymer in many aerospace applications. It is expected that 3D-printed LCP will get considerable attention and adoption in the next future thanks to its outstanding characteristics when properly printed. If, for any reason, our selection had been limited to non-metallic candidates, LCP would have been the best choice. PEI is another plastic material of interest for aerospace applications. It has been exploited for the realisation of a CubeSat structure in the ReD-SHIFT project, providing some interesting advantages in terms of weight (Becedas et al., 2018; Rossi et al., 2019). However, in our analysis PEI shows a rather poor performance with respect to both lightness and demisabilty.

Material charts reported in this work are based on values for properties of conventional materials, i.e. produced by standard fabrication techniques. It is worth noting that the mechanical properties of 3D-printed material can differ significantly from conventionally produced parts (Bourell et al., 2017; Hanzl et al., 2015). The same usually does not happen for other functional properties, like the thermal ones for example. The effect of lowering mechanical properties is to increase the indexes M1 and M2, which are proportional to the inverse of the square root of the Young modulus. If we took PEEK as example, it has been reported that its mechanical properties are reduced upon fabrication by additive manufacturing (Wu et al., 2015). 3D-printed parts possess a modulus of elasticity that is 50% lower than the injection moulded samples. This would shift the coordinates of PEEK in our material chart as shown in Fig. 4a, further distancing the material from the optimal ones. While it is almost impossible to quantify a priori the exact reduction of mechanical properties due to additive manufacturing, for the best candidates we referenced to values that have already been reported in literature. Our analysis suggests that even if the material presents the appropriate values of mechanical and thermal properties, the fabrication process must always be considered as it may influence sensibly the final selection, up to the point to push the material outside the acceptable range.

Fig. 4b shows the trade-off surface (dashed line) of our selection. As we mentioned before, no material presents simultaneously the lowest *M1* and *M2* and thus our choice is not straightforward. The trade-off surface defines the subset of solutions that offer the best compromise between the two objectives. We define the relative penalty function Z^* as an aggregate of our objectives, normalized over the values of reference (indicated by the "*0*" subscript).

$$Z^* = \alpha_m{}^* \frac{m}{m_0} + \alpha_Q{}^* \frac{Q}{Q_0}$$

$$\frac{m}{m_0} = \left(\frac{\rho}{E^{\frac{1}{2}}}\right)\left(\frac{E_0^{\frac{1}{2}}}{\rho_0}\right)$$

$$\frac{Q}{Q_0} = \left[\frac{\rho c_p\left(T_f - T_0\right) + \rho\lambda_m}{E^{\frac{1}{2}}}\right]\left[\frac{E_0^{\frac{1}{2}}}{\rho_0 c_{p,0}\left(T_{f,0} - T_0\right) + \rho_0\lambda_{m,0}}\right]$$

$$\alpha = \frac{\alpha_m{}^*}{\alpha_Q{}^*}$$

The terms on the right of the first equation represent the ratio of the material indexes and the reference indexes, while $\alpha_m{}^*$ and $\alpha_Q{}^*$ are the exchange constants and they measure the decrease in penalty for a fractional decrease in mass or heat, all other parameters kept constant. These exchange constants are dimensionless and their ratio, α, indicates how much we value one performance index over the other. If, for example, we set $\alpha = 10$, meaning that lightness is much more highly valued than heat to decom-

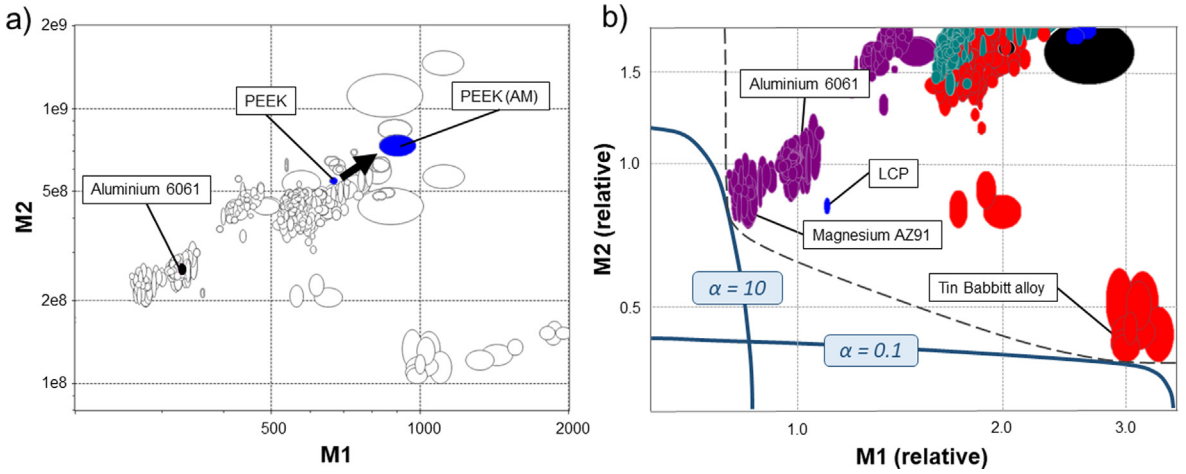

Fig. 4. a) An example of the effect of additive manufacturing on PEEK: the limited Young modulus after FDM (reported by Wu et al. 2015), causes the material to drift towards larger values of M1 and M2. The label PEEK identifies the material produced by conventional injection moulding, while the label PEEK (AM) indicates the additive manufactured polymer. Note that if a material is close to the optimal choices, this effect can cause it to be discarded from the selection. b) Trade-off surface (dashed line) related to the multiple objectives selection of our investigation. Each bubble is a material that meets the constraints, but only candidates close to the trade-off surface are non-dominated solutions and thus represent the best choices. The two solid curves are penalty functions calculated with specific values of the exchange constants. The contour that is tangent to the trade-off surface identifies the optimum solution: in the plot, magnesium alloys when $\alpha = 10$ and tin alloys when $\alpha = 0.1$.

position, the contour blue line, identifying Z^*/α_m, would be tangent to the trade-off surface in a specific point in the chart, and the most attractive candidates are the one nearest to this point. Magnesium alloys, in this case, would be our preferential choice. If, instead, we valued heat to decomposition more than lightness, setting $\alpha = 0.1$, the most attractive choice would become tin alloys. These are interesting candidates for secondary structures, like balancing masses, that are critical for demisability (Riley et al., 2017). Tin alloys present densities similar to steel, which is usually selected for this type of auxiliary components, thus representing a valid alternative. It is worth noting that, when the two objectives are equally considered, not only magnesium AZ91 but also LCP are better choices compared to aluminium 6061. Table 3 displays values of the penalty function for three different exchange constant combinations referred to three of the most attractive candidates. The final selection depends on the context and the relative importance of the two objectives: for aerospace applications, usually, mass reduction is one of the most valued parameters. Mass is strongly associated to the cost for launching to orbit, so the implications of this objective are quite clear. Without a new regulation from space agencies, it is difficult to find the drive to sacrifice mass over other objectives due to the potential increase in the total cost of the mission. Keeping in mind all these considerations, magnesium alloys seem to be the most attractive candidates for the objectives of our research.

The final step of the selection process is focused on seeking documentation, which can confirm the availability and effectiveness of the real materials. Recent research and progress made on Mg alloys, tin alloys, and LCP supports our rationale and our results, especially when considering the capacity to 3D-print these materials (Gantenbein et al., 2018; Hsieh et al., 2016; Salehi et al., 2019). Studies have demonstrated that our best candidates can be 3D-printed avoiding the mechanical properties reduction due to the fabrication process. For example, it has been reported that LCP, thanks to molecular domains orientation during printing, can present stiffness, strength and toughness comparable to (or even larger than) the standard material properties (Gantenbein et al., 2018). Tin Babbitt alloy can be produced by Fused Filament Fabrication (FFF) in specimen which possess ultimate strength, yield strength and elongation matching the ones of the conventionally manufactured metal (Warrier and Kate, 2018). Magnesium alloy (particularly AZ91) have been successfully 3D-printed with properties that resemble the strength of casted magnesium alloy (Karunakaran et al., 2020; Wei et al., 2014). These examples corroborate the effectualness of our findings. Nevertheless, more investigation have yet to be performed to reliably obtain 3D-printed parts with the desired mechanical properties, limiting the reduction caused by improper printing conditions (Bourell et al., 2017; Lee et al., 2017; Ngo et al., 2018; Popescu et al., 2018).

Table 3
Values for Z^*/α_m for the reference material and three of the best candidates, evaluated with different combinations of the exchange constants. Minimum value of the penalty function are in bold. Tin alloys become attractive choices only when the heat to decomposition objective is valued much more than the lightness objective. When the two performances are equally considered, magnesium AZ91 and LCP are better candidates than aluminium 6061.

Material	$\alpha = 10$	$\alpha = 1$	$\alpha = 0.1$
Aluminium, 6061 T6	1.1	2.0	11.0
Magnesium, AZ91	**0.9**	**1.7**	9.4
LCP	1.2	1.9	9.3
Tin, Babbitt Metal Alloy 3	3.0	3.5	**8.1**

4. Conclusions

The increasing number of CubeSats being developed and used for scientific, technological and commercial applications poses several concerns about the multiplication of space debris in LEO and the associated potential collision on Earth's surface during uncontrolled re-entry. Among a multitude of potential solutions for this problem, recurring to cost-effective and reliable systems in the framework of design for demise can contribute to the mitigation of space debris. We proposed a novel selection of materials for the structural bus of CubeSats with the intent of identifying alternative options that can easily melt during atmospheric re-entry, thus reducing the likelihood of an impact on the Earth's surface. Our analysis identified magnesium alloys as an optimal choice, as they provide a mass reduction and less heat to demise during re-entry compared to the reference material aluminium 6061 T6. Another potential candidate is LCP: it has a slightly lower performance related to the mass metric, but it can decompose with less heat than both aluminium 6061 and the majority of magnesium alloys. Its particularity is that it is the only plastic material among the best choices. Tin alloys are the most demisable materials among our selection, but they present a large mass index and thus become the optimum only if weight-reduction were not important, an unlikely scenario for aerospace applications. Nonetheless, tin alloys are an interesting choice for secondary components like balancing masses or, whenever possible, reaction wheels. In this case, the high demisability of such materials can be an advantage in spacecraft design. Furthermore, we reported that the best candidates in our investigation can actually be fabricated by additive manufacturing, preserving their mechanical properties and thus in accordance to the results of our selection process. Our findings provide innovative solutions in terms of material selection, favouring the exploitation of additive manufacturing techniques for commercial space applications and contributing to the development of in-orbit production for space exploration and colonisation.

5. Fundings

This research has been funded by the "Higher Education and Development" program (code FP1619892003, channel 1420AFPLO2) by European Social Fund.

Declaration of Competing Interest

The authors declare the following financial interests/personal relationships which may be considered as potential competing interests: [A. G. has filed patent application IT201700091364A1 relating to this work.].

Appendix A. Supplementary material

Supplementary data to this article can be found online at https://doi.org/10.1016/j.asr.2020.11.037.

References

Akyildiz, I.F., Kak, A., 2019. The internet of space things/CubeSats: A ubiquitous cyber-physical system for the connected world. Comput. Networks 150, 134–149. https://doi.org/10.1016/j.comnet.2018.12.017.

Barsoum, G.I., Ibrahim, H.H., Fawzy, M.A., 2019. Static and random vibration analyses of a university CubeSat project. J. Phys. Conf. Ser. 1264. https://doi.org/10.1088/1742-6596/1264/1/012019.

Bastida Virgili, B., Dolado, J.C., Lewis, H.G., Radtke, J., Krag, H., Revelin, B., Cazaux, C., Colombo, C., Crowther, R., Metz, M., 2016. Risk to space sustainability from large constellations of satellites. Acta Astronaut. 126, 154–162. https://doi.org/10.1016/j.actaastro.2016.03.034.

Becedas, J., Caparrós, A., Ramírez, A., Morillo, P., Sarachaga, E., Martín-Moreno, A., 2018. Advanced Space Flight Mechanical Qualification Test of a 3D- Printed Satellite Structure Produced in Polyetherimide ULTEMTM, in: Advanced Engineering Testing. InTech, p. 38. https://doi.org/10.5772/intechopen.79852

Beck, J.C., Holbrough, I., Schleutker, T., Guelhan, A., 2019. Improved representation of destructive spacecraft re-entry from analysis of high enthalpy wind tunnel tests of spacecraft and equipment. Acta Astronaut. 164, 287–296. https://doi.org/10.1016/j.actaastro.2019.07.033.

Bourell, D., Kruth, J.P., Leu, M., Levy, G., Rosen, D., Beese, A.M., Clare, A., 2017. Materials for additive manufacturing. CIRP Ann. - Manuf. Technol. 66, 659–681. https://doi.org/10.1016/j.cirp.2017.05.009.

Burleigh, S.C., De Cola, T., Morosi, S., Jayousi, S., Cianca, E., Fuchs, C., 2019. From connectivity to advanced internet services: a comprehensive review of small satellites communications and networks. Wirel. Commun. Mob. Comput. 2019. https://doi.org/10.1155/2019/6243505.

California Polytechnic State University, 2014. CubeSat Design Specification Rev. 13. CubeSat Program, Calif. Polytech. State 22.

Carandente, V., Savino, R., 2014. New concepts of deployable de-orbit and re-entry systems for CubeSat miniaturized satellites. Recent Patents Eng. 8, 2–12. https://doi.org/10.2174/1872212108666140204004335.

Chen, S., Bourham, M., Rabiei, A., 2014. Novel light-weight materials for shielding gamma ray. Radiat. Phys. Chem. 96, 27–37. https://doi.org/10.1016/j.radphyschem.2013.08.001.

Ehrenfreund, P., Ricco, A.J., Squires, D., Kitts, C., Agasid, E., Bramall, N., Bryson, K., Chittenden, J., Conley, C., Cook, A., Mancinelli, R., Mattioda, A., Nicholson, W., Quinn, R., Santos, O., Tahu, G., Voytek, M., Beasley, C., Bica, L., Diaz-Aguado, M., Friedericks, C., Henschke, M., Landis, D., Luzzi, E., Ly, D., Mai, N., Minelli, G., Mclntyre, M., Neumann, M., Parra, M., Piccini, M., Rasay, R., Ricks, R., Schooley, A., Stackpole, E., Timucin, L., Yost, B., Young, A., 2014. The O/OREOS mission-astrobiology in low earth orbit. Acta Astronaut. 93, 501–508. https://doi.org/10.1016/j.actaastro.2012.09.009.

Espalin, D., Muse, D.W., MacDonald, E., Wicker, R.B., 2014. 3D Printing multifunctionality: Structures with electronics. Int. J. Adv. Manuf. Technol. 72, 963–978. https://doi.org/10.1007/s00170-014-5717-7.

European Cooperation for Space Standardization, 2012. Space Engineering - Testing. ECSS Stand.

European Cooperation for Space Standardization, 2008. Structural general requirements. ECSS Stand. 134.

Gantenbein, S., Masania, K., Woigk, W., Sesseg, J.P.W., Tervoort, T.A., Studart, A.R., 2018. Three-dimensional printing of hierarchical liquid-crystal-polymer structures. Nature 561, 226–230. https://doi.org/10.1038/s41586-018-0474-7.

Gaudenzi, P., Atek, S., Cardini, V., Eugeni, M., Graterol Nisi, G., Lampani, L., Pasquali, M., Pollice, L., 2018. Revisiting the configuration of small satellites structures in the framework of 3D Additive Manufacturing. Acta Astronaut. 146, 249–258. https://doi.org/10.1016/j.actaastro.2018.01.036.

Grim, B., Kamstra, M., Ewing, A., Nogales, C., Griffin, J., Parke, S., 2016. MakerSat: a CubeSat designed for in-space assembly. Conf. small Satell. 30, 9.

Gutierrez, C., Salas, R., Hernandez, G., Muse, D., Olivas, R., MacDonald, E., Irwin, M.D., Wicker, R., Newton, M., Church, K., 2011. CubeSat fabrication through additive manufacturing and micro-dispensing, in: International Symposium on Microelectronics. International Microelectronics Assembly and Packaging Society, pp. 1021–1027.

Hakima, H., Bazzocchi, M.C.F., Emami, M.R., 2018. A deorbiter CubeSat for active orbital debris removal. Adv. Sp. Res. 61, 2377–2392. https://doi.org/10.1016/j.asr.2018.02.021.

Hanzl, P., Zetek, M., Bakša, T., Kroupa, T., 2015. The influence of processing parameters on the mechanical properties of SLM parts. Procedia Eng. 100, 1405–1413. https://doi.org/10.1016/j.proeng.2015.01.510.

Hsieh, P.C., Tsai, C.H., Liu, B.H., Wei, W.C.J., Wang, A.B., Luo, R.C., 2016. 3D printing of low melting temperature alloys by fused deposition modeling. Proc. IEEE Int. Conf. Ind. Technol. 2016-May, 1138–1142. https://doi.org/10.1109/ICIT.2016.7474915

Inter-Agency Space Debris Coordination Committee, 2007. Space Debris Mitigation Guidelines.

Kang, S.-J., Oh, H.-U., 2016. On-Orbit Thermal Design and Validation of 1 U Standardized CubeSat of STEP Cube Lab. Int. J. Aerosp. Eng. 2016, 1–17. https://doi.org/10.1155/2016/4213189.

Karunakaran, R., Ortgies, S., Tamayol, A., Bobaru, F., Sealy, M.P., 2020. Additive manufacturing of magnesium alloys. Bioact. Mater. 5, 44–54. https://doi.org/10.1016/j.bioactmat.2019.12.004.

Kelley, R.L., Jarkey, D., 2015. In: CubeSat Material Limits For Design for Demise, in. American Institute of Aeronautics and Astronautics, Reston, Virginia. https://doi.org/10.2514/6.2015-4671.

Klinkrad, H., Beltrami, P., Hauptmann, S., Martin, C., Sdunnus, H., Stokes, H., Walker, R., Wilkinson, J., 2004. The ESA Space Debris Mitigation Handbook 2002. Adv. Sp. Res. 34, 1251–1259. https://doi.org/10.1016/j.asr.2003.01.018.

Lee, J.Y., An, J., Chua, C.K., 2017. Fundamentals and applications of 3D printing for novel materials. Appl. Mater. Today 7, 120–133. https://doi.org/10.1016/j.apmt.2017.02.004.

Murtaza, A., Pirzada, S.J.H., Xu, T., Jianwei, L., 2020. Orbital Debris Threat for Space Sustainability and Way Forward (Review Article). IEEE Access 8, 61000–61019. https://doi.org/10.1109/ACCESS.2020.2979505.

NASA Goddard Space Flight Center, 2013. General Environmental Verification Standard (GEVS).

Ngo, T.D., Kashani, A., Imbalzano, G., Nguyen, K.T.Q., Hui, D., 2018. Additive manufacturing (3D printing): A review of materials, methods, applications and challenges. Compos. Part B Eng. 143, 172–196. https://doi.org/10.1016/j.compositesb.2018.02.012.

Okolie, A.C., Onuh, S.O., Olatunbosun, Y.T., Abolarin, M.S., 2016. Design Optimization of Pico-satellite Frame for Computational Analysis and Simulation. Am. J. Mech. Ind. Eng. 1, 74–84. https://doi.org/10.11648/j.ajmie.20160103.17

Peral, E., Im, E., Wye, L., Lee, S., Tanelli, S., Rahmat-Samii, Y., Horst, S., Hoffman, J., Yun, S.H., Imken, T., Hawkins, D., 2018. Radar Technologies for Earth Remote Sensing from CubeSat Platforms. Proc. IEEE 106, 404–418. https://doi.org/10.1109/JPROC.2018.2793179.

Piattoni, J., Candini, G.P., Pezzi, G., Santoni, F., Piergentili, F., 2012. Plastic Cubesat: An innovative and low-cost way to perform applied space research and hands-on education. Acta Astronaut. 81, 419–429. https://doi.org/10.1016/j.actaastro.2012.07.030.

Popescu, D., Zapciu, A., Amza, C., Baciu, F., Marinescu, R., 2018. FDM process parameters influence over the mechanical properties of polymer specimens: A review. Polym. Test. 69, 157–166. https://doi.org/10.1016/j.polymertesting.2018.05.020.

Prater, T.J., Werkheiser, M.J., Jehle, A., Ledbetter, F., Bean, Q., Wilkerson, M., Soohoo, H., Hipp, B., 2017. NASA's In-Space Manufacturing Project: Development of a Multimaterial Fabrication Laboratory for the International Space Station, in: AIAA SPACE and Astronautics Forum and Exposition. American Institute of Aeronautics and Astronautics, Reston, Virginia. https://doi.org/10.2514/6.2017-5277

Quiroz-Garfias, C., Silva-Navarro, G., Rodríguez-Cortés, H., 2007. Finite element analysis and design of a CubeSat class picosatellite structure. 2007 4th Int. Conf. Electr. Electron. Eng. ICEEE 2007, 294–297. https://doi.org/10.1109/ICEEE.2007.4345026.

Riley, D., Fuentes, I.P., Meyer, J.C., Proffe, G., Lips, T., Beyer, F., Soares, T., 2017. Design for demise: Systems-level techniques to reduce re-entry casualty risk. Proc. Int. Astronaut. Congr. IAC 6, 3633–3645.

Rossi, A., Alessi, E.M., Schettino, G., Beck, J., Holbrough, I., Schleutker, T., Letterio, F., de Miguel, G.V., Becedas Rodríguez, J., Dalla Vedova, F., Stokes, H., Colombo, C., Gkolias, I., Bernelli Zazzera, F., Miguel, N., Walker, S., Romei, F., Tsiganis, K., Skoulidou, D.K., Stoll, E., Schaus, V., Popova, R., Kim, Y., Francesconi, A., Olivieri, L., Gerardin, S., 2019. The H2020 Redshift project: A successful European effort towards space debris mitigation. Proc. Int. Astronaut. Congr. IAC 2019-Octob.

Rossi, A., Colombo, C., Tsiganis, K., Beck, J., Rodriguez, J.B., Walker, S., Letterio, F., Vedova, F.D., Schaus, V., Popova, R., Francesconi, A., Stokes, H., Schleutker, T., Alessi, E.M., Schettino, G., Gkolias, I., Skoulidou, D.K., Holbrough, I., Zazzera, F.B., Stoll, E., Kim, Y., 2018. ReDSHIFT: A global approach to space debris mitigation. Aerospace 5, 1–15. https://doi.org/10.3390/aerospace5020064.

Salehi, M., Maleksaeedi, S., Nai, M.L.S., Gupta, M., 2019. Towards additive manufacturing of magnesium alloys through integration of binderless 3D printing and rapid microwave sintering. Addit. Manuf. 29. https://doi.org/10.1016/j.addma.2019.100790 100790.

Schoolcraft, J., Klesh, A., Werne, T., 2016. MarCO: Interplanetary mission development on a cubesat scale. SpaceOps 2016 Conf. 1–8. https://doi.org/10.2514/6.2016-2491.

Selva, D., Krejci, D., 2012. A survey and assessment of the capabilities of Cubesats for Earth observation. Acta Astronaut. 74, 50–68. https://doi.org/10.1016/j.actaastro.2011.12.014.

Shiroma, W.A., Martin, L.K., Akagi, J.M., Akagi, J.T., Wolfe, B.L., Fewell, B.A., Ohta, A.T., 2011. CubeSats: A bright future for nanosatellites. Cent. Eur. J. Eng. 1, 9–15. https://doi.org/10.2478/s13531-011-0007-8.

Stevenson Soler Chisabas, R., Loureiro, G., de Oliveira Lino, C., Cantor, D.F., 2017. Method for CubeSat Thermal-Vacuum Cycling Test Specification, in: 47th International Conference on Environmental Systems. pp. 1–15.

Straub, J., Marsh, R., Kerlin, S., 2015. The use of additive manufacturing for CubeSat design and testing, in: Third Annual North Dakota Space Robotics Forum.

Sweeting, M.N., 2018. Modern Small Satellites-Changing the Economics of Space. Proc. IEEE 106, 343–361. https://doi.org/10.1109/JPROC.2018.2806218.

Toorian, A., Diaz, K., Lee, S., 2008. The CubeSat approach to space access. IEEE Aerosp. Conf. Proc. 1. https://doi.org/10.1109/AERO.2008.4526293.

Warrier, N., Kate, K.H., 2018. Fused filament fabrication 3D printing with low-melt alloys. Prog. Addit. Manuf. 3, 51–63. https://doi.org/10.1007/s40964-018-0050-6.

Wei, K., Gao, M., Wang, Z., Zeng, X., 2014. Effect of energy input on formability, microstructure and mechanical properties of selective laser melted AZ91D magnesium alloy. Mater. Sci. Eng. A 611, 212–222. https://doi.org/10.1016/j.msea.2014.05.092.

Woellert, K., Ehrenfreund, P., Ricco, A.J., Hertzfeld, H., 2011. Cubesats: Cost-effective science and technology platforms for emerging and developing nations. Adv. Sp. Res. 47, 663–684. https://doi.org/10.1016/j.asr.2010.10.009.

Wu, W., Geng, P., Li, G., Zhao, D., Zhang, H., Zhao, J., 2015. Influence of layer thickness and raster angle on the mechanical properties of 3D-printed PEEK and a comparative mechanical study between PEEK and ABS. Materials (Basel). 8, 5834–5846. https://doi.org/10.3390/ma8095271.